ISSN 0915-633X

NATIONAL INSTITUTE FOR FUSION SCIENCE

Liquid Stub Tuner for Ion Cyclotron Heating

R. Kumazawa, T. Mutoh, T. Seki, F. Shinpo, G. Nomura, T. Ido,
T. Watari, Jean-Marie Noterdaeme and Yangping Zhao

(Received - Dec. 25, 1998)

NIFS-585 Feb. 1999

RESEARCH REPORT
NIFS Series

NAGOYA, JAPAN

Liquid Stub Tuner for Ion Cyclotron Heating

R.Kumazawa, T.Mutoh, T. Seki, F.Sinpo, G.Nomura, T.Ido, T.Watari,
Jean-Marie Noterdaeme* and Yangping Zhao**

National Institute for Fusion Science
**Max-Planck-Institut fuer Plasmaphysik*
***Academia Sinica Plasma Physics Institute*

Abstract

Ion Cyclotron Range of Frequency (ICRF) heating on the Large Helical Device (LHD) is characterized by high power (up to 12MW) and steady state operation (30 minutes). The LHD is a helical device (with a major radius of 3.9m and a minor radius of 0.6m) with super-conducting coil windings (l=2, m=10). The main purpose of physical research is to investigate currentless and disruption-free plasma. Research and development for steady state ICRF heating has been carried out in recent years: A high RF power transmission system consisting of stub tuners, a ceramic feed-through and an ICH loop antenna has been developed. In addition, steady state operation of an RF oscillator has been achieved at a power higher than 1MW.

A liquid stub tuner has been proposed as an innovation. The liquid stub tuner makes use of the difference between the RF wave lengths in liquid and in gas due to the different relative dielectric constants. The liquid stub tuner has been experimentally proved to be a reliable RF component for high power transmission systems. Test results have quantitatively demonstrated that it can be used at high RF voltage: 61kV for 10 seconds and 50kV for 30 minutes. Furthermore, the liquid surface can be shifted under high RF voltage without breakdown, which suggests that it can be employed as a feedback control impedance matching tool to keep reflected RF power at a low level with regard to a temporal variation of plasma loading resistance.

Keywords: liquid stub tuner, ICRF heating, feedback control, high power/steady state heating

I. INTRODUCTION

Research and development for heating in the Ion Cyclotron Range of Frequency (ICRF) in steady state at high power has been carried out at the National Institute for Fusion Science. The LHD is a helical device (with a major radius of 3.9m and a minor radius of 0.6m) with super-conducting coil windings (l=2, m=10), and the main purpose is to investigate currentless and disruption-free plasma[1-4]. The initial plasma experiment was conducted using 2nd harmonic electron cyclotron heating (ECH, 84GHz) at a magnetic field strength 1.5T, in 1998[5,6]. In the next experimental cycle, neutral beam injection (NBI) heating and ICRF heating will be applied to the ECH plasma. ICRF heating will be applied to the LHD plasma in two heating scenarios: at 12MW for several seconds and in a steady state at 3MW. Research and development have been carried out since 1993. First, an RF oscillator system with a wide frequency range was designed and fabricated. The ICRF heating includes various heating methods such as two-ion-hybrid heating, minority heating, ion Bernstein wave (IBW) heating and higher harmonic heating. Since the experimental magnetic field strength will change from 1T to 4T, the frequency range has been determined to be from 25 to 95MHz. The RF oscillator can be operated in a steady state (for 5,000 seconds) at 1.6MW by finding a low impedance mode to reduce the screen grid current and ion current in the tetrode tube[7]. In parallel with the development of the RF oscillator, an RF power transmission system has been developed, which consists of stub tuners, a ceramic feed-through, a DC break and an ICRF heating loop antenna. The ceramic feed-throughs of a cone shaped type and of a cylindrical silicon nitride (Si_3N_4) ceramic can tolerate steady state operation at 40kV[8,9]. The whole system for RF power

transmission can be operated in a steady state at 40kV[7]. If the plasma loading resistance is assumed to be 5Ω, the transmission line has the capability to deliver 1.6MW of RF power to the LHD plasma.

In tokamak experiments, ICRF heating is now accepted as a reliable heating tool. In Heliotron and Stellarator systems, however, ICRF heating has not always demonstrated successful heating[10-12]. ICRF-heated plasma has often suffered from impurity problems. Recently ICRF heating has been successfully applied in Compact Helical System (CHS)[13-16] and Wendelstein (W-7AS)[17-19].

An L-H mode transition and an ELMy plasma have prevented ICRF heating from being applied in high RF power with a long pulse, due to an increase in reflected RF power, as observed in many tokamak experiments. On JIPP T-II U, L-H mode transitions have been observed above a threshold RF power, followed by ELMs. At the transition between L- and H-modes, some of the RF oscillators cease to transmit RF power, injected power becomes about half and the plasma returns to L-mode immediately[20]. On JET, the problem has been solved by a radial plasma position feedback control, where the overall response time is typically 0.1s [21,22].

On TEXTOR and Tore Supra, feedback control can be done using variable capacitors controlled by computer in the impedance matching circuit[23. 24]. Experiments have succeeded in keeping the reflected power at a low level by this method, at a typical response time of 0.1sec in 1MW power operation. However, the life time of the capacitors is dependent on their movable speed and acceleration. A 3 dB coupler is also useful for presenting a constant impedance matching to the oscillator in the presence of rapidly varying plasma loading such as due to EMLs[25-27].

Recently a new idea concerning feedback control using a ferrite core has been proposed, and research and development has just started[28]. This method utilizes the non-linearity of the magnetic permeability of the ferrite. The method is now under development for D-IIID and will be tested on ASDEX-UG. Typical response time is about 1ms. In high RF power operation. RF power dissipation due to ferrite hysteresis may lead to a temperature increase even if the ferrite is cooled by water.

We have surveyed the present status of ICRF heating and feedback control impedance matching methods. It is indispensable to develop a reliable stub tuner for steady state operation that has the capability of feedback control. ICRF heating in LHD must heat the plasma at high power (up to 12MW) and in a steady state (30 minutes). Therefore, it is important for the impedance matching to follow a temporal variation of the LHD plasma loading resistance.

In this paper, a liquid stub tuner is proposed as an innovation. A liquid stub tuner is superior to a conventional stub tuner because it has no sliding contact. Therefore, it is important to demonstrate that the liquid stub tuner can withstand a high RF voltage in long pulse operation and that its surface can be shifted during the application of high RF voltage without RF breakdown. Typical response time may not be fast enough to respond to L-H transition; however, the liquid stub tuner will be useful in ICRF heating experiments at high RF power. The principle and the characteristics of the liquid stub tuner will be explained in Sec.II. In Sec.III, the experimental setup will be described. In Sec.IV, experimental results are given. In Sec.V. we will discuss experimental data and an advanced method.

II. LIQUID STUB TUNER

A. Conceptual Design of a Liquid Stub Tuner

A liquid stub tuner is proposed as a new component of an impedance matching circuit. The impedance matching circuit is located between the ICRF heating antenna and the RF oscillator and generally consists of a conventional stub tuner, a liquid stub tuner and a phase shifter. The liquid stub tuner contains a liquid as shown in Fig.1. Its use is based on the difference between the RF wave lengths in liquid and in gas due to the different relative dielectric constants. The liquid stub tuner is able to be used as a conventional stub tuner by changing the liquid surface level without shifting the electrical shortend. Needless to say, impedance matching is always attained by shifting the shortends of conventional stub tuners and/or by changing the length of the phase shifter. It is, however, dangerous to move the shortend of the stub tuner or the sliding joint of the phase shifter during high power ICRF heating, because 1kA of RF current flows there in MW level heating. Therefore a liquid stub tuner will be superior to the conventional one.

A function of the liquid stub tuner is illustrated in Fig.1. RF voltage is V_1 and RF currents at the T-junction are I_1 and I_2, respectively. RF current, I' flows to the liquid stub tuner and RF current is I_t at the shortend of the liquid stub tuner. The relation between V_1, I' and I_t is formulated in the following equation;

$$\begin{pmatrix} V_1 \\ I \end{pmatrix} = \begin{pmatrix} \cos 2\pi A_{GS} & jZ_0 \sin 2\pi A_{GS} \\ j/Z_0 \sin 2\pi A_{GS} & \cos 2\pi A_{GS} \end{pmatrix} \begin{pmatrix} \cos 2\pi A_{LS} & jZ_L \sin 2\pi A_{LS} \\ j/Z_L \sin 2\pi A_{LS} & \cos 2\pi A_{LS} \end{pmatrix} \begin{pmatrix} 0 \\ I_t \end{pmatrix}$$

$$\begin{pmatrix} V_1 \\ I \end{pmatrix} = \begin{pmatrix} E & jF \\ jG & H \end{pmatrix} \begin{pmatrix} 0 \\ I_t \end{pmatrix} \qquad (1)$$

RF voltage and RF current on the liquid surface can be calculated using the second matrix and the RF parameters (RF voltage, 0 and RF current, I_t) at the shortend in eq. (1). Z_L and A_{LS} are the characteristic impedance and the length normalized by RF wave length in the liquid, respectively. RF voltage and RF current at the T-junction can be calculated using the first matrix and the RF parameters on the liquid surface. Z_0 and A_{GS} are the characteristic impedance of a coaxial transmission line and the length normalized by RF wave length in the gas region, respectively. Components of the matrix E, F,G and H are as follow:

$E = \cos 2\pi A_{GS} \cos 2\pi A_{LS} - Z_0/Z_L \sin 2\pi A_{GS} \sin 2\pi A_{LS}$
$F = Z_L \cos 2\pi A_{GS} \sin 2\pi A_{LS} + Z_0 \sin 2\pi A_{GS} \cos 2\pi A_{LS}$
$G = 1/Z_0 \sin 2\pi A_{GS} \cos 2\pi A_{LS} + 1/Z_L \cos 2\pi A_{GS} \sin 2\pi A_{LS}$
$H = -Z_L/Z_0 \sin 2\pi A_{GS} \sin 2\pi A_{LS} + \cos 2\pi A_{GS} \cos 2\pi A_{LS}$

I' is calculated by eliminating I_t in the following equation;

$$I' = -jH / FV_1 \qquad (2)$$

RF current, I' obeys Kirchhoff's law at the T-junction. Therefore

$$I_1 = I' + I_2 = -jH / FV_1 + I_2 \qquad (3)$$

On the other hand, the relation between the RF voltage and current in a conventional stub tuner is expressed as follows;

$$\begin{pmatrix} V_1 \\ I_1 \end{pmatrix} = \begin{pmatrix} 1 & 0 \\ -j/Z_0/\tan 2\pi A_S & 1 \end{pmatrix} \begin{pmatrix} V_1 \\ I_2 \end{pmatrix} \qquad (4)$$

We derive the relation between the liquid and the conventional stub tuners by using eqs.(3) and (4) in the following equation,

$$\frac{1}{\tan 2\pi A_S} = \frac{1 - Z_L/Z_0 \tan 2\pi A_{GS} \tan 2\pi A_{LS}}{\tan 2\pi A_{GS} + Z_L/Z_0 \tan 2\pi A_{LS}} \qquad (5)$$

Figure 2 shows the calculated results of eq.(5) for 3 liquid stub tuners of different lengths, where the relative dielectric constant of the liquid is $\varepsilon_L = 2.72$. Ratios of the characteristic impedance and the RF wave length are $Z_L/Z_0 = \varepsilon_L^{-1/2}$ and $\lambda_L/\lambda_0 = \varepsilon_L^{-1/2}$ in eq.(5). The abscissa is a ratio of the liquid height to the total length of the liquid stub tuner, and the ordinate shows how the liquid stub tuner behaves like a conventional stub tuner A_S, as formulated in eq.(5). When the normalized length of the liquid stub tuner is $A_0 = 0.3$, the variable range of the liquid stub tuner is from 0.3 to 0.5. When the liquid stub tuner is short in the normalized length, $A_0 = 0.1$, it does not work as a stub tuner. The operating range becomes wider with the liquid stub tuner length.

B. Fabrication of Liquid Stub Tuner

To test the liquid stub tuner concept, a 260cm long liquid stub tuner has been fabricated, consisting of a 104mm inner copper conductor and a 240mm outer aluminum conductor, as shown in Fig.3. Cooling water flows inside the inner conductor and the outer conductor is surrounded by a water-cooled copper tube. Silicon oil (Dimethyl Polysiloxane) is used as the liquid. It has been selected because of the low vapor pressure and the low dielectric loss. The vapor pressure is less than 0.1torr even at 240°C. The dielectric constant, ε_L is 2.72 and the dielectric loss tangent, $\tan\delta$ is 10^{-4} to 3.3×10^{-4} in the frequency range of 10-100MHz (at 25°C), as shown in Table.1. The temperature dependence of $\tan\delta$ is known to be small from 0°C to 100°C at 50Hz; however, it is not known how $\tan\delta$ increases with liquid temperature in the frequency range (25-95MHz). This will be discussed in Section IV.E. The liquid surface level can be shifted by the use of an oil pump and valves, as shown in Fig.3. The speed of motion of the liquid surface is 0.5cm/sec. The liquid stub tuner is equipped with electrostatic probes to measure RF voltage and a thermocouple to measure the liquid temperature. At the top of the liquid stub tuner, a gas stop has been installed to isolate it from other transmission lines.

III. EXPERIMENTAL SETUP

A schematic drawing of the R&D experimental setup is shown in Fig.4. The RF oscillator system consists of three stages of amplifiers: IPA (4kW), DPA (100kW) and FPA (2MW). The final amplifier (FPA) is composed of a 4m long double-coaxial cavity, which makes it possible to tune in the frequency range of 25-95MHz. It has the capability of transmitting 2MW for several seconds and more than 1.5MW in a steady state.

High RF power operations of 2MW in 10 seconds and 1.6MW in steady state have been achieved at 50MHz.

In this experimental setup, RF power was transmitted to a dummy load or R&D experimental setup through a co-axial switch. The experimental setup was sometimes changed (as described later), so this system was very convenient. An RF power of several W was applied to the R&D experimental setup from one port of the co-axial switch. An impedance matching is acquired by adjusting positions of the liquid surface and the conventional stub tuner. The RF oscillator was tuned to maximize power at the frequency for which the system was matched.

A double stub tuner system has been adopted as an impedance matching circuit. The transmission system consists of 240mm coaxial transmission line components, whose characteristic impedance is 50Ω and which are in the same configuration as the liquid stub tuner. Cooling water flows inside the inner conductor for steady state RF power operation. The stub tuner on the RF oscillator side is a conventional one with a sliding contact. The liquid stub tuner has been arranged on the RF antenna side in the double stub tuner system as shown in Fig.4. At the beginning of the R&D experiment, a conventional stub tuner was used there; however, it was damaged in steady state operation at a relatively low RF voltage (20kV). An RF current of about 400A made a hole in the outer conductor at the movable sliding contact. A mechanism actuated by an air cylinder was adopted in the movable sliding contact. When it is moved, the tight contact is relieved by pressurized air. In spite of careful design and fabrication, a conventional stub tuner could not withstand steady state operation even at a relatively low RF voltage: So it has been replaced with a liquid stub tuner. A conventional stub tuner did not cause a serious problem on the RF oscillator side, as the RF current was much smaller there than on the antenna side. A pre-matching stub tuner was located near a ceramic feed-through in order to reduce the RF standing wave. The RF voltage could be reduced to 30% between the pre-matching stub tuner and the impedance matching circuit in the selected situation. Experimental data will be described in detail elsewhere. The performance of the ceramic feed-through is another matter of the greatest importance for high-power and steady state ICRF heating, the R&D results of which are described in other papers[8,9]. In a vacuum tank, a test R&D loop antenna was installed, which was a proto-type antenna 430mm wide and 630mm long.

A liquid stub tuner was placed on the antenna side of a double stub tuner system. The liquid stub tuner was connected to a T junction through elbows and a straight transmission line as shown in Fig.4. The total length was 6.5m. The height of the liquid surface could be changed from 0m to 2.2m, so that 34% of the whole length could be filled with liquid. According to eq.(5), the normalized operating length of the liquid stub tuner can be calculated in Fig.5 in two cases of 40MHz and 50MHz. From this figure, the liquid stub tuner works from 0.85 to 1.05 and from 1.05 to 1.3 in the normalized length in f= 40MHz and 50MHz, respectively.

RF power was transmitted to the impedance matching circuit and the RF antenna through the coaxial switch and DC break in the transmission system. When the transmission system can withstand a high RF voltage, a large RF power can be transferred. Therefore a high RF voltage test of each RF component is required. How much RF power can be delivered to the RF antenna is deduced by a following equation.

$$P_{RF} = \frac{1}{2} R \left(\frac{V_{RF}}{50}\right)^2 \qquad (6)$$

When the maximal RF voltage, V_{RF} is 40kV or 45kV of standing wave, the power transmission capability is estimated to be P_{RF}=1.6MW or 2MW for the case of the plasma loading resistance of R=5Ω, respectively. The final goal of this R&D was the achievement of 40kV for 30minutes and 45kV for 10seconds at the transmission system. Here the RF loading resistance was R=0.4Ω because of the absence of plasma, so that a relatively low RF power, e.g. 128-162kW, could attain a high RF voltage as stated above. The above-mentioned goals were achieved[7]; however, higher RF voltage tests were sometimes interrupted by vacuum pressures higher than 1×10^{-5} torr. In this case the transmission system was disconnected from the antenna at point A as shown in Fig.4 to increase the test RF voltage in the liquid stub tuner.

IV. EXPERIMENTAL RESULTS

A. Frequency Feedback Control for High RF Voltage and Long Pulse Test

The reflected RF power was increased with time on a long pulse test of the liquid stub tuner. A typical experimental result is shown in Fig.6(a). In this figure, the time evolutions of forward RF power P_{fw}, reflected power P_{ref}, and RF voltage V_{RF} are shown in the case of the absence of frequency feedback control. Here RF voltage means the maximal voltage in the standing wave. RF voltages were measured at several positions between the RF antenna and the impedance matching circuit. The maximal RF voltage was determined by fitting measured RF voltages to the standing wave distribution using the value of Voltage Standing Wave Ratio (VSWR). RF voltage was measured by an electrostatic probe inserted from a port attached to the outer conductor. In this

operation, the RF voltage was 22.5kV at the beginning of the pulse; however, it decreased to 16kV with the increase in reflected RF power. At the end of the RF pulse at 50sec, the reflected power fraction P_{ref}/P_{fw} exceeded 50%. The RF power supply would have been discontinued to protect a tetrode tube in the final amplifier by an interlock system which was not used in this experiment. Figure 6(b), on the other hand, shows typical operation using a frequency feedback control, where the same forward RF power is applied as in Fig.6(a). In this operation, the reflected power fraction could be kept less than 1% by a change of frequency from 42.02MHz to 41.95MHz. In this case the RF voltage was constant at V_{RF}=22.5kV. Here the required frequency change, df/f was 0.2% in 50seconds operation. When the higher RF power was applied, the required df/f increased and the modulation rate became faster. The optimal frequency became almost constant after a few minutes.

The cause may be attributed to thermal expansion of the transmission lines in radial and axial directions. Looking for indirect evidence, we examined the dependence of the frequency in impedance matching on the deformation of the transmission line using a pressurized gas. The shift of the impedance matched frequency was measured while changing the filling pressure of nitrogen gas from a vacuum to 4kg/cm^2. This experimental result shows how the frequency changes with the filling pressure. The frequency shift can be explained by the increase in the characteristic impedance and the expansion in the transmission line. However, quantitative assessment has not been done to explain the phenomena.

B. RF Voltage Distribution in Liquid

It is important to measure the RF voltage in the liquid. By measuring RF voltage distribution, the RF wave length has been found to be shorter in the liquid due to the fact that the relative dielectric constant is larger than one. The RF voltage measurement method used was the same as that described before; however, it should be noted that the RF voltage was observed to be larger by a factor of the relative dielectric constant, ε_L =2.72 in the liquid. Figure 7 shows a typical RF voltage distribution in the liquid and in the nitrogen gas (4kg/cm^2) in the case of a peak RF voltage of 61.3kV and a frequency of 41MHz. Needless to say, the RF voltage in the liquid was confirmed to be the same as that between the antenna and the impedance matching circuit. The liquid surface was found to be 112cm measured from the bottom of the liquid stub tuner. The RF wave length in the liquid was λ_L = 4.4m, which was shorter than that in the gas, λ_0 = 7.3m. The shortening rate agreed with the reciprocal of the square root of the relative dielectric constant of the liquid, $\lambda_l/\lambda_0=\varepsilon_L^{-1/2}$. Furthermore, the position of the maximal RF voltage was located just at the liquid surface. Recalling eq.(5) and Fig.5, it was found that the derivative of the resultant normalized length A_s could be made largest in this situation.

C. Operational Regime on High RF Voltage and Duration Time

It is an important matter how high an RF voltage V_{RF} and how long a time the liquid stub tuner can withstand without RF breakdown. Two criteria were set up to decide whether the liquid stub tuner can be used or not as an RF component in our ICRF heating system: Whether it could endure V_{RF}=45kV for 10seconds and 40kV for 30minutes. The duration times of 10seconds and 30minutes were selected as typical of a short pulse and of steady state ICRF heating on LHD. RF voltages of 45kV and 40kV are equivalent to a transmission capability of heating RF power, 2MW and 1.6MW for the plasma loading resistance 5Ω, respectively. In the normal experimental setup as shown in Fig 4, the operation time is often limited by the increase in vacuum pressure, which is caused by multipactoring discharge. When the vacuum pressure increases to more than 1×10^{-5} torr, RF breakdown occurs in the whole vacuum chamber and the impedance can not be matched. The vacuum condition is improved well by aging the RF antenna. Both the two criteria described above were achieved, i.e. V_{RF}=58kV for 10 seconds and V_{RF}=40kV for 30 minutes, respectively.

To test the liquid stub tuner at a higher RF voltage than these values, the transmission line was disconnected at point A as shown in Fig.4 to remove the influence of the increased vacuum pressure. Figure 8 shows results achieved so far in RF voltage and duration time. 61.3kV and 50kV have been achieved for 10 seconds and 30 minutes operation, respectively. In this test, no RF breakdown has been observed. The capability of RF power transmission is calculated to be 3.75MW for 10 seconds and 2.5MW for 30 minutes for the LHD plasma loading resistance 5Ω. It was decided to adopt the liquid stub tuner as a reliable stub tuner for the impedance matching circuit of ICRF heating on LHD.

D. Liquid Movement Test during High RF Voltage Operation

In the previous section, the reliable performance of the liquid stub tuner in a steady state at high RF voltage was described. Here it is reported whether the liquid stub tuner can be a feedback control tool to respond to temporal variation of the plasma loading resistance during long pulse or steady state ICRF

heating. To verify its feasibility for use as a feedback control in impedance matching, the liquid surface was moved to reduce the reflected RF power fraction at V_{RF}=46kV operation as shown in Fig.9. The reflected RF power fraction 12% could be reduced to almost 0% within half second by shifting the liquid surface by 2.7mm. The velocity of the liquid surface movement was 0.5cm/sec. In this experiment, the loading resistance was less than 1Ω and the circuit Q value was high, so that a liquid surface shift of several mm restored the reflected RF power fraction to a negligible level. During ICRF heating on the LHD plasma, however, the plasma loading resistance will be larger by one order of magnitude than the present value, so that the required liquid surface shift may exceed several cm. We will have to develop a system equipped with a mechanism which can move the liquid surface faster.

E. Temperature Increase in Liquid with Steady State Operation

In high RF voltage operation, Ohmic loss on the inner and outer conductors amounts to a considerable quantity. The average loss is estimated at a few kW/m in the case of V_{RF}=40-50kV. With a liquid stub tuner, the dissipated power due to the liquid dielectric loss must also be added to the Ohmic loss. The temperature increase in the liquid was examined during high RF voltage operation for long pulse. A thermocouple was installed by replacing an RF voltage probe in a measurement port. A typical example of the time evolution of the liquid temperature is shown in Fig.10. The RF power was applied at V_{RF}=40kV for 30 minutes. At the beginning of this shot, the liquid temperature increased linearly with time. At the end of the operation, however, the temperature tended to saturate. The maximal temperature increase was 26°C as shown in Fig.10. A series of experiments was carried out to measure the liquid temperature increase at various applied RF voltages. Figure 11 shows the dependence of the liquid temperature increase on RF voltage at 30 minutes operation in two cases, where the inner conductors (solid lozenges) and both conductors (solid circles) were cooled by water. The liquid temperature increase is proportional to $V_{RF}^{1.5}$. In Fig.11, the average temperature increase in the case of a thermally insulated liquid is also plotted with a dashed line; this will be discussed in the next section (V.B).

Concerning RF dielectric loss in the liquid, the temperature effect on dielectric loss tanδ was examined. Some materials have the characteristic that tanδ increases and dielectric loss increases non-linearly with the temperature. It may be possible to predict that tanδ does not increase with the liquid temperature by recalling the experimental results shown in Figs.10 and 11. That the liquid tanδ does not increase with the temperature was verified in another way. The RF loading resistance was measured, changing the liquid temperature from 20°C to 60°C. The loading resistance was of the order of 0.1Ω, because the RF antenna and the transmission line were disconnected in this experiment. These data are plotted in Fig.12. The measured loading resistance data were almost constant and concentrated at $0.103 \pm 0.0024\Omega$ over a wide temperature range. Here the loading resistance mainly comes from the Ohmic loss on the surfaces of the outer and inner conductors and the RF dielectric loss in the liquid. When the RF dielectric loss in the liquid 4.2kW at V_{RF}=40kV is used (discussed later in Sec.V.A), the fraction of the loading resistance due to it is calculated to be 0.013Ω. If the liquid tanδ doubled, we would have been able to observe an increase in the measured loading resistance. Figures 12 shows that the non-linear increase in tanδ is very small.

V. DISCUSSION

A. Calculation of RF Power Dissipation in Liquid

In this section, RF power dissipation in the liquid is calculated. The radial RF electric field E(r,z) can be formulated in radial and axial directions r and z when RF voltage V_{RF} is applied between the inner and outer conductors with radii of a and b, respectively.

$$E(r,z) = \frac{V_{RF}}{\ln(b/a)}\frac{1}{r}\sin(\frac{2\pi}{\lambda_L}z) \qquad (7)$$

The RF power dissipation due to dielectric loss P_L can be calculated by integrating in radial and axial directions using the relative dielectric constant ε_L, a dielectric loss tangent of the liquid tanδ and the RF wave length λ_l in the liquid.

$$P_L = \frac{1}{2}\varepsilon_0\varepsilon_L \tan\delta\omega\int_0^z\int_a^b 2\pi r E^2(r,z)drdz$$
$$= \pi\varepsilon_0\varepsilon_L \tan\delta\omega\frac{V_{RF}^2}{\ln(b/a)}(\frac{1}{2}z - \frac{\lambda_L}{8\pi}\sin(\frac{4\pi}{\lambda_L}z)) \qquad (8)$$

As described in the previous section (III.B), the liquid surface position is located at a quarter of the RF wave length as shown in Fig.7. Then P_L is

$$P_L = \frac{\pi}{8}\lambda_L\varepsilon_0\varepsilon_L \tan\delta\omega\frac{V_{RF}^2}{\ln(b/a)} \qquad (9)$$

When λ_L=4.44m, ε_0=8.85×10^{-12}, ε_L=2.72, tanδ=2×10^{-4}, ω/2π=41MHz, and ln(b/a)=0.83, P_L is calculated to

be 4.2kW at V_{RI}=40kV. When the plasma loading resistance is 5Ω, the RF transmitted power is 1.6MW at V_{RI}= 40kV and the ratio of the liquid dielectric loss to the transmitted RF power is 4.2kW/1,600kW=0.27%.

B Liquid Temperature Increase

The liquid temperature increase can be deduced by using the above-mentioned dissipated RF power, which is proportional to a square of V_{RI} according to eq.(9) When the liquid is assumed to be thermally insulated, the dependence of average temperature increase T_{liq} on RF voltage can be calculated using a liquid heat capacity of 0.36cal/g with the following equation:

$$T_{liq}(^{\circ}C) = 0.07\ V_{RI}{}^{2}(kV) \qquad (10)$$

The calculated values are plotted in a dashed line as shown in Fig.11. The liquid temperature increase is 120°C in the case of V_{RF}= 40kV, if the liquid is not cooled. Recalling the vapor pressure of the liquid, it is less than 0.001torr at this temperature, which is a low enough vapor pressure in nitrogen gas (4kg/cm^2).

C. Feedback Control in Impedance Matching

The experiment concerning shifting the liquid surface was described in a previous section (IV.D). The response time is half a second; however the typical duration of the H-L mode transition is less than 1ms. Feedback control in an impedance matching circuit based on a liquid stub tuner does not have the ability to respond to a quick transition. A frequency feedback control method using a twin stub tuner in a double stub tuner system has been proposed[29]. This method has a response time of less than 1ms; it has been tested at a low RF power level using virtual electrical resistance instead of the plasma loading resistance. The weak point of the frequency feedback control is that output RF power of the oscillator deteriorates if the frequency is moved far from the central frequency. For example, RF output decreases by 23% in the frequency modulation of +-0.4% at an RF power level of 1MW in our RF oscillator. The required frequency modulation depends on how much the plasma loading resistance changes. It was thought that the best impedance matching circuit for LHD would be equipped with a liquid stub tuner and frequency feedback control system. This method has not yet been applied to a plasma with a high RF power of 1MW; however, future experiments will prove the validity of a liquid stub tuner used in combination with a frequency feedback control.

This technological research and development should be important in helping to achieve high RF power heating or current drive in steady state operation on LHD and future devices such as ITER.

ACKNOWLEDGMENTS

The authors wish to thank Profs. A.Iiyoshi, M Fujiwara, O Motojima and K.Ohkubo for their helpful discussion and support.

REFERENCES

1) A.Iiyoshi, K.Yamazaki, Physics of Plasmas, 2(6), 2349 (1995).
2) O.Motojima, K.Akaishi et al., Fusion Engineering and Design, 20, 3(1993).
3) M.Fujiwara, K.Yamazaki et. al., Journal of Fusion Engineering, Vol.15, Nos.1/2, 7(1996).
4) O.Motojima et. al., IAEA-F1-CN-69, FT1/2(1998).
5) A.Iiyoshi et. al., IAEA-F1-CN-69, OV1/4(1998).
6) M.Fujiwara et. al., IAEA-F1-CN-69, EX2/3(1998).
7) R.Kumazawa, T.Mutoh et al., Proceeding of 18th Symposium on Fusion Technology, Vol.1, 617(1996).
8) T.Mutoh , R.Kumazawa et al., Fusion Engineering and Design, 26, 387(1995).
9) T.Mutoh T, R.Kumazawa et al., to be published in Fusion Engineering and Design.
10) T.Mutoh et. al., Nuclear Fusion 24, 1003(1984).
11) M.Balico et. al., AIP Conf. Proc. 224, 150(1992).
12) M.Kwon et.al., Nuclear Fusion 32, 1225(1992).
13) R.Kumazawa, K.Nishimura et al., Proceeding of 21st European Conference, Vol, 1, 1000(1994).
14) K.Nishimura, R.Kumazawa et al., Proc. 15th International Conference on Plasma Physics and Controlled Nuclear Fusion Research, Vol.1, 783(1994).
15) S.Masuda, R.Kumazawa et.al., Nuclear Fusion, Vol.37, 53(1997).
16) T.Watari, R.Kumazawa et al., 12th Topical Conference on Radio Frequency Power in Plasmas, 57(1997).
17) J.M.Noterdaeme et.al., Proc. 16th International Conference on Fusion Energy, Vol.3, 335(1996),
18) D.A.Hartmann, G.Cattanei et al., 12th Topical Conference on Radio Frequency Power in Plasma, 49(1997).
19) D.A.Hartmann, G.Cattanei, IAEA-F1-CN-69, CD1/5(1998).
20) T.Watari, R.Kumazawa et al., Nuclear Fusion, Vol.30, 1197(1990).
21) V.P.Bhatnagar et al., Proc. 18th European Conference, Vol.1, 367(1991).
22) The JET team presented by J.Jacquinot, Plasma physics and Controlled Fusion Vol.33, No.13, 1675(1991).
23) F.Durodie and M.Vervier, Proceeding of 17th Symposium on Fusion Technology, Vol.1, 477(1992).
24) L.Ladurelle et. al., Proceeding of 19th Symposium on Fusion Technology, Vol.1, 593(1996).

25) R.H.Goulding et. al., 11th Topical Conference on Radio Frequency Power in Plasma, 397(1995).
26) R.I.Pinsker et.al., 12th Topical Conference on Radio Frequency Power in Plasma, 393(1997).
27) J.-M. Noterdaeme et. al., IAEA-F1-CN-69, CDP11(1998).
28) F.Braun and J.deGrassie, in private communication.
29) R.Kumazawa, T.Mutoh et. al., Proceeding of 17th Symposium on Fusion Technology, Vol.1, 554(1992).

Table Captions

Table.1 Characteristics of Dimethyl Polysiloxane

Relative Dielectric Constant	Dielectric Loss Tangent	Vapor Pressure	Specific Heat
2.72	1×10^{-4} at 10MHz 3.3×10^{-4} at 100MHz	0.04torr at 240°C 2torr at 320°C	0.36

Table 2. Experimentally Achieved Results in Liquid Stub Tuner

Duration Time	RF Voltage at 0.4Ω	Capability of Transmission RF Power at Plasma Resistance, 5Ω	Liquid Temperature Increase
10 seconds	61.3kV	3.8MW	-
30 minutes	50kV	2.5MW	35°C

Figure Captions

Fig.1 Schematic drawing of liquid stub tuner. Liquid stub tuner is connected at T-junction of transmission line. End is electrically terminated.

Fig.2 Operating length in liquid stub tuner on variable liquid surface height for 3 cases of normalized length, A_0=0.1, 0.2 and 0.3.

Fig.3 Schematic drawing of liquid stub tuner with RF voltage measured ports, consisting of 240mm of coaxial transmission line. Liquid surface height can be changed by pump and valves.

Fig.4 Layout of ICRF heating test stand system for testing liquid stub tuner. RF power is transmitted from final amplifier to R&D test section through co-axial switch and D.C.break. Liquid stub tuner is located at antenna side in impedance matching system, which consists of a double stub tuner. To test in high RF voltage, transmission line is disconnected at A.

Fig.5 Operating length in liquid stub tuner on variable liquid surface height for 2 cases of 40MHz and 50MHz.

Fig.6 (a) Time evolution of RF power, reflected power and RF voltage without frequency feedback control in 40kW operation. (b) Time evolution of RF power, reflected power, RF voltage and frequency with frequency feedback control.

Fig.7 RF voltage distribution in liquid stub tuner in 61.3kV operation. Liquid surface level is located at 112cm.

Fig.8 RF voltage and pulse length achieved in liquid stub tuner for 10seconds and 30minutes operations.

Fig.9 Reduction of reflected RF power fraction by shifting liquid surface height in operation of RF voltage, 46kV.

Fig.10 Time evolution of liquid temperature increase in 40kV/30min operation.

Fig.11 Dependence of liquid temperature increase on RF applied voltage in cases of no cooling(in calculation), inner transmission line with water cooling, and both transmission lines with water cooling.

Fig.12 Dependence of RF loading resistance on liquid temperature.

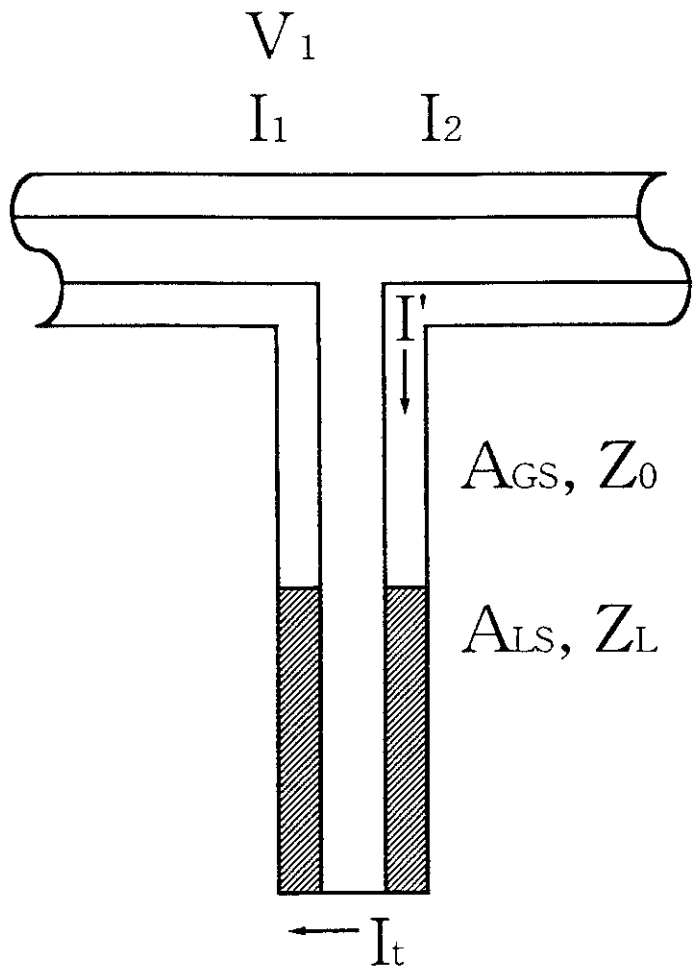
V1
I1
I2
I'
AGS, Z0
ALS, ZL
It

Fig. 1

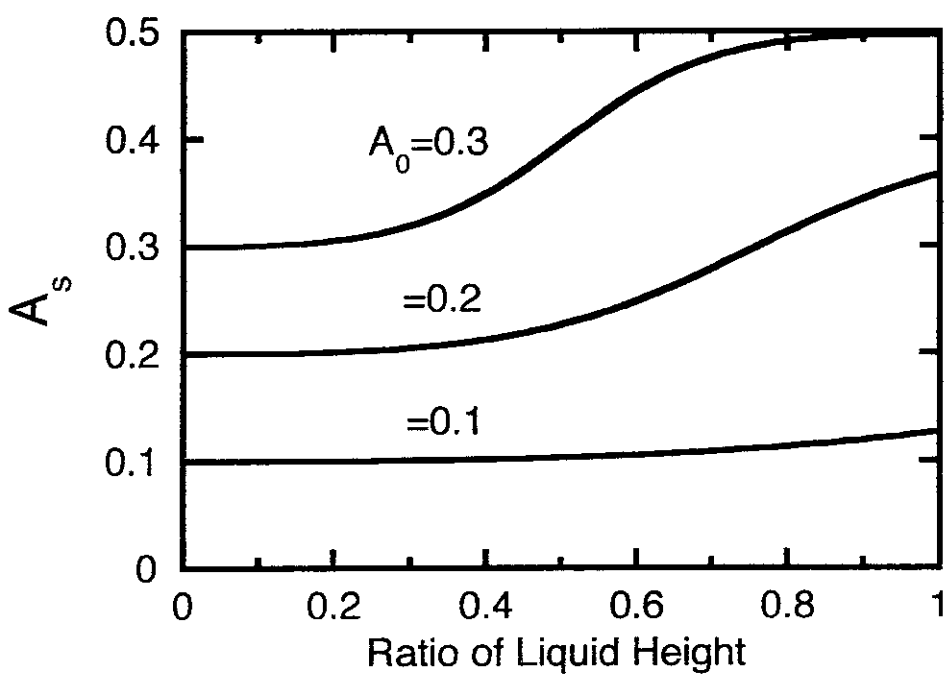
0.5
0.4
0.3
0.2
0.1
0
A0=0.3
=0.2
=0.1
As
0
0.2
0.4
0.6
0.8
1
Ratio of Liquid Height

Fig. 2

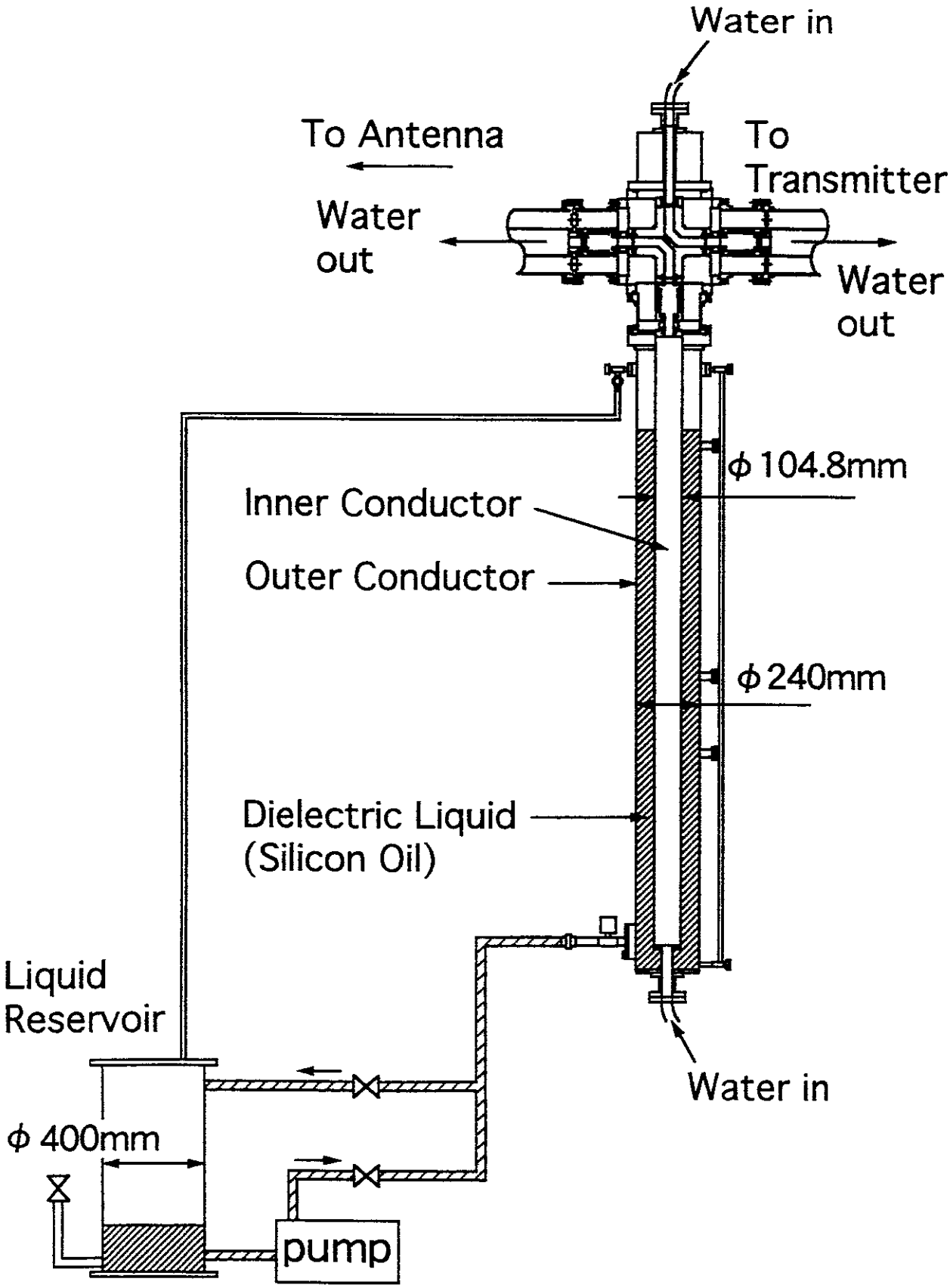
Water in
To Antenna
To
Transmitter
Water
out
Water
out
ϕ 104.8mm
Inner Conductor
Outer Conductor
ϕ 240mm
Dielectric Liquid
(Silicon Oil)
Liquid
Reservoir
Water in
ϕ 400mm
pump

Fig. 3

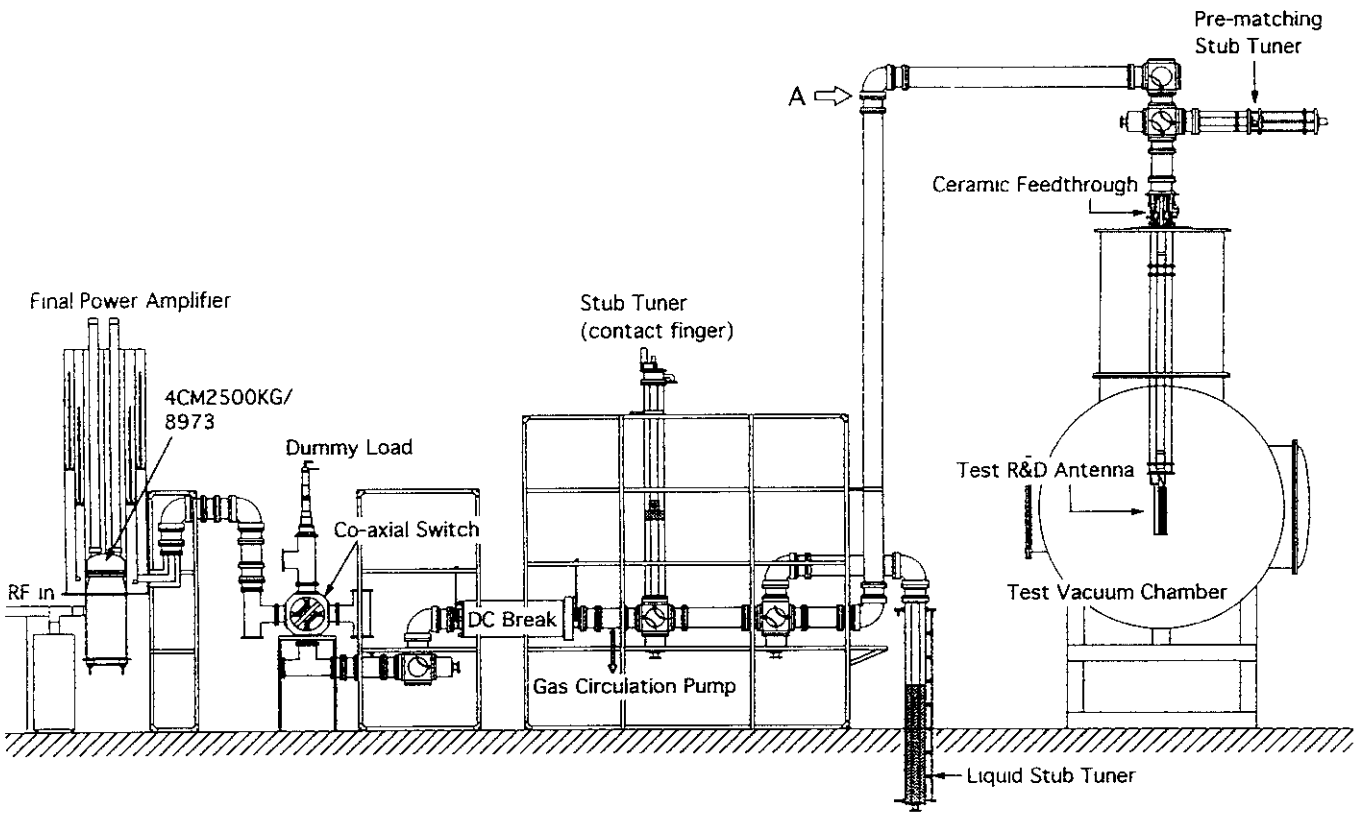
Pre-matching
Stub Tuner
A
Ceramic Feedthrough
Final Power Amplifier
4CM2500KG/
8973
Dummy Load
Stub Tuner
(contact finger)
Test R&D Antenna
Co-axial Switch
RF in
DC Break
Test Vacuum Chamber
Gas Circulation Pump
Liquid Stub Tuner

Fig. 4

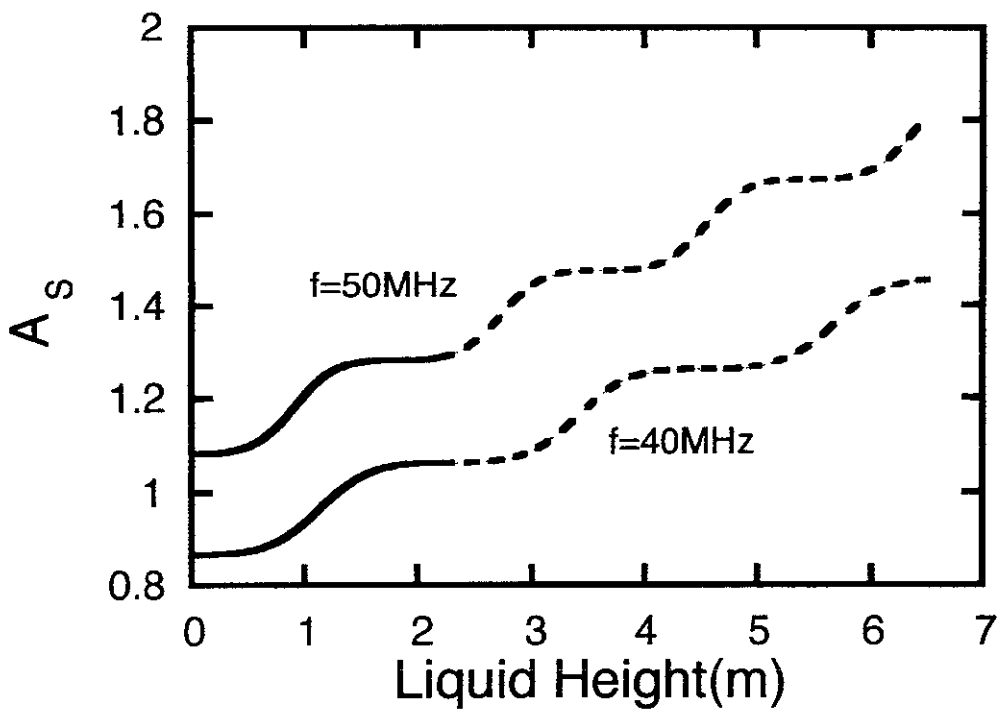
2
1.8
1.6
1.4
1.2
1
0.8
A_S
f=50MHz
f=40MHz
0
1
2
3
4
5
6
7
Liquid Height(m)

Fig. 5

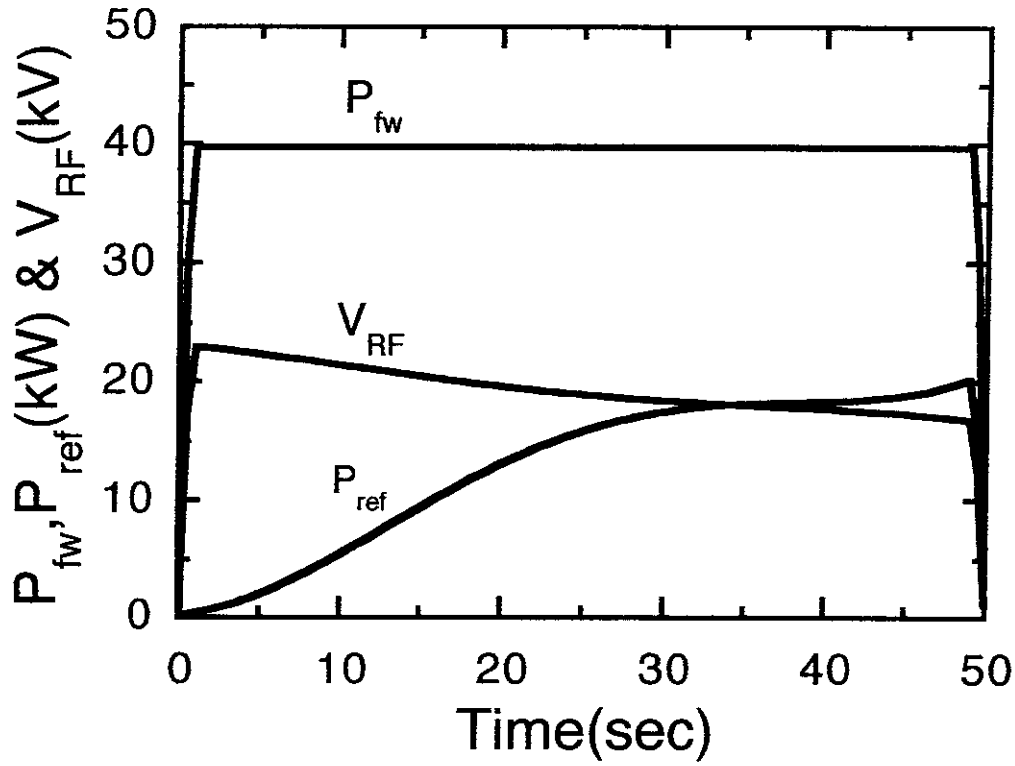
50
40
30
20
10
0
P_{fw}
V_{RF}
P_{ref}
P_{fw}, P_{ref}(kW) & V_{RF}(kV)
0
10
20
30
40
50
Time(sec)

Fig. 6 (a)

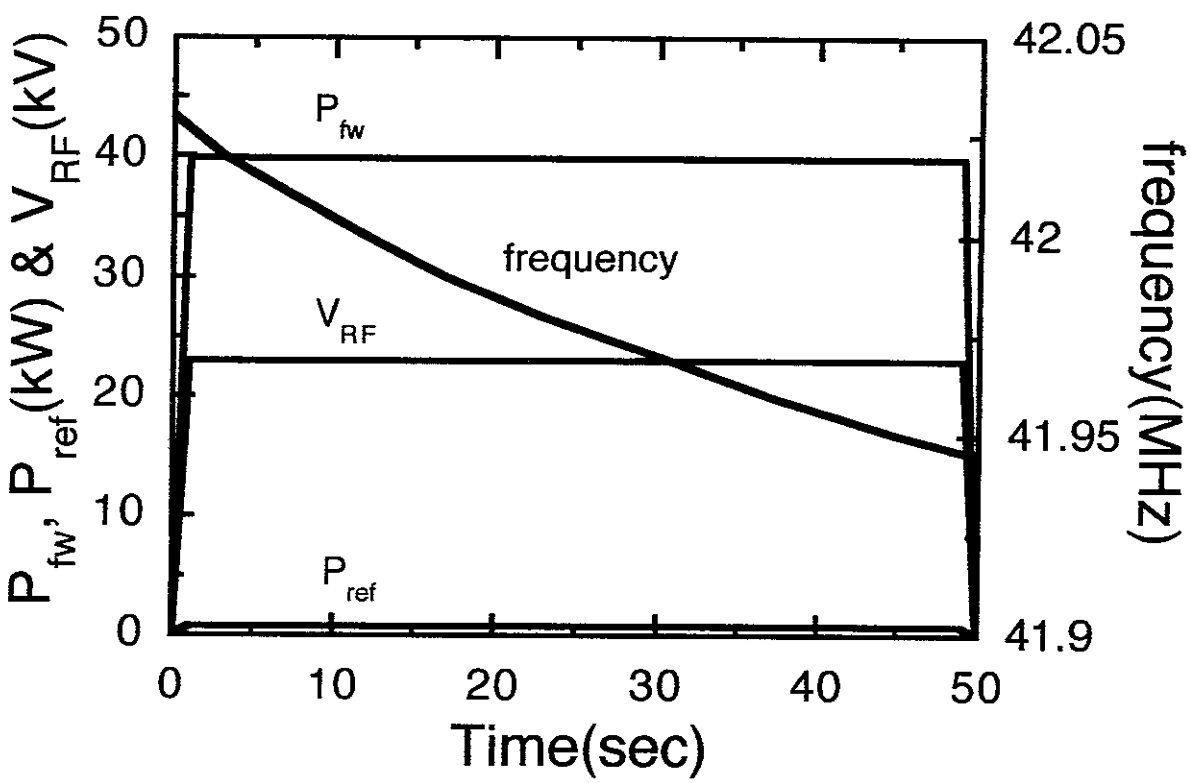
50
40
30
20
10
0
P_{fw}
frequency
V_{RF}
P_{ref}
P_{fw}, P_{ref}(kW) & V_{RF}(kV)
42.05
42
41.95
41.9
frequency(MHz)
0
10
20
30
40
50
Time(sec)

Fig. 6 (b)

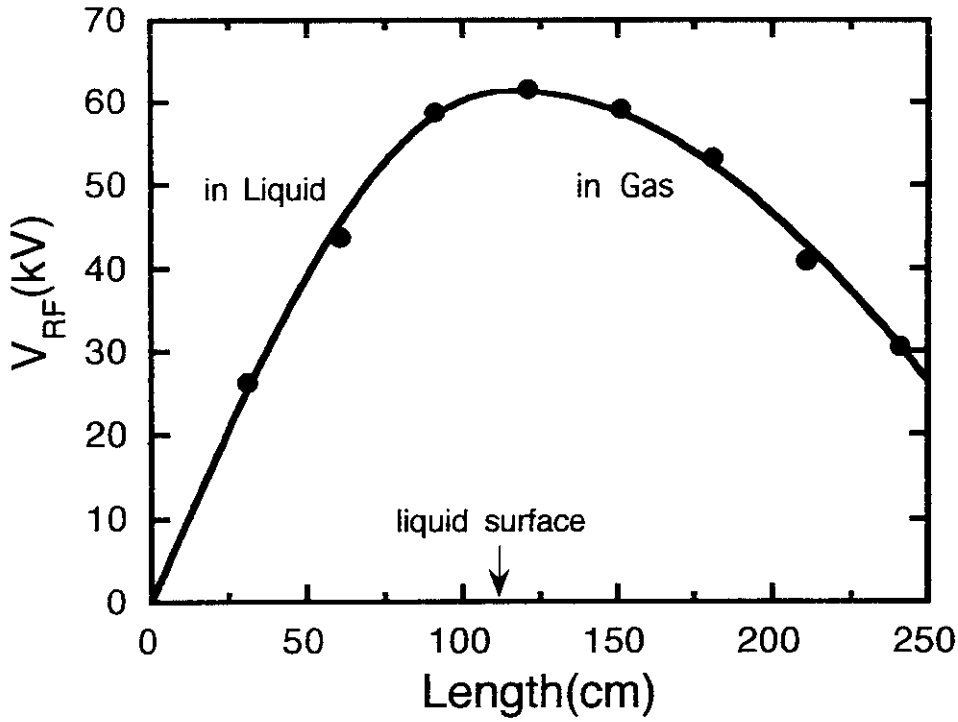
70
60
50
40
30
20
10
0
V_{RF}(kV)
in Liquid
in Gas
liquid surface
0
50
100
150
200
250
Length(cm)

Fig. 7

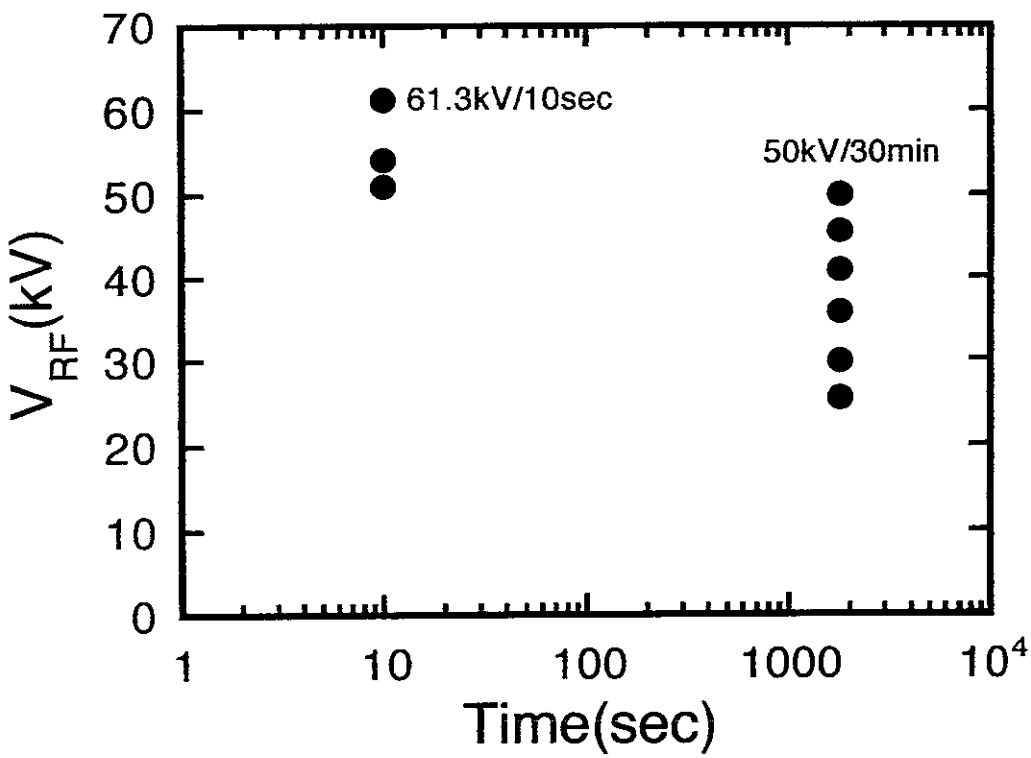
70
60
50
40
30
20
10
0
V_{RF}(kV)
61.3kV/10sec
50kV/30min
1
10
100
1000
10^4
Time(sec)

Fig. 8

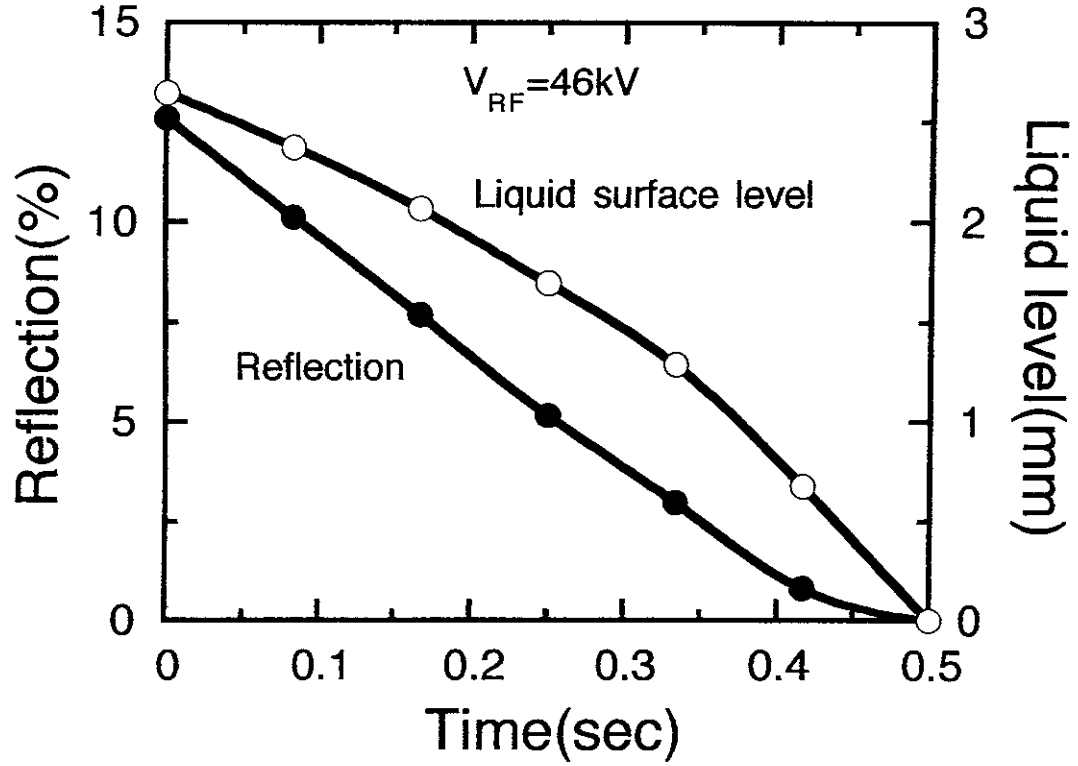
15
10
5
0
3
2
1
0
0
0.1
0.2
0.3
0.4
0.5
V_{RF}=46kV
Liquid surface level
Reflection
Reflection(%)
Liquid level(mm)
Time(sec)

Fig. 9

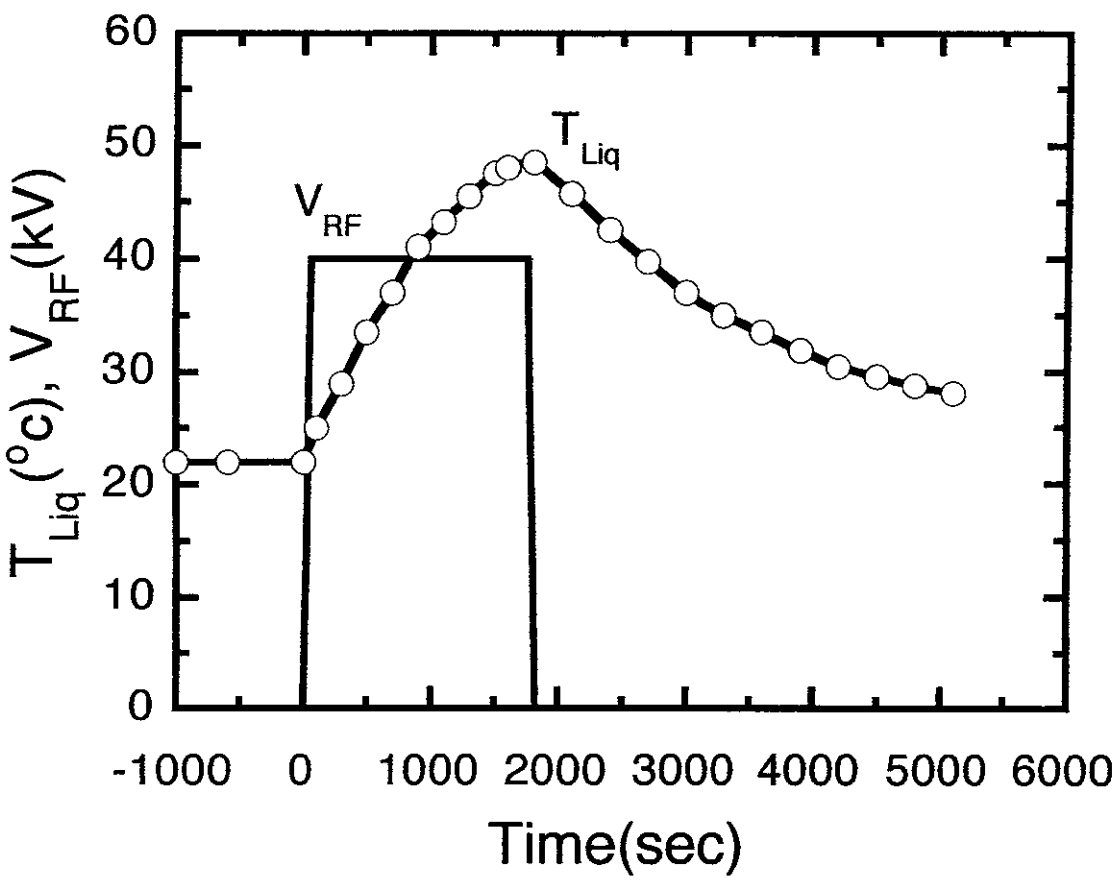
60
50
40
30
20
10
0
T_{Liq}
V_{RF}
T_{Liq}(^{o}c), V_{RF}(kV)
-1000
0
1000
2000
3000
4000
5000
6000
Time(sec)

Fig. 10

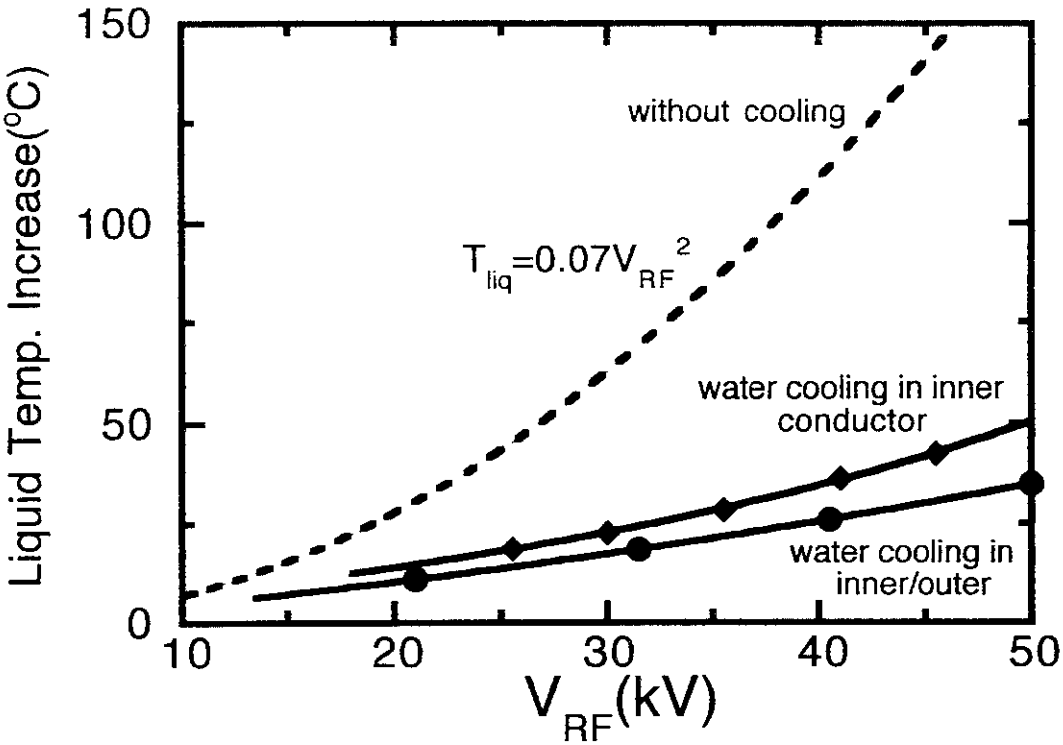
150
100
50
0
Liquid Temp. Increase(°C)
without cooling
$T_{liq}=0.07V_{RF}^{2}$
water cooling in inner conductor
water cooling in inner/outer
10
20
30
40
50
V_{RF}(kV)

Fig. 11

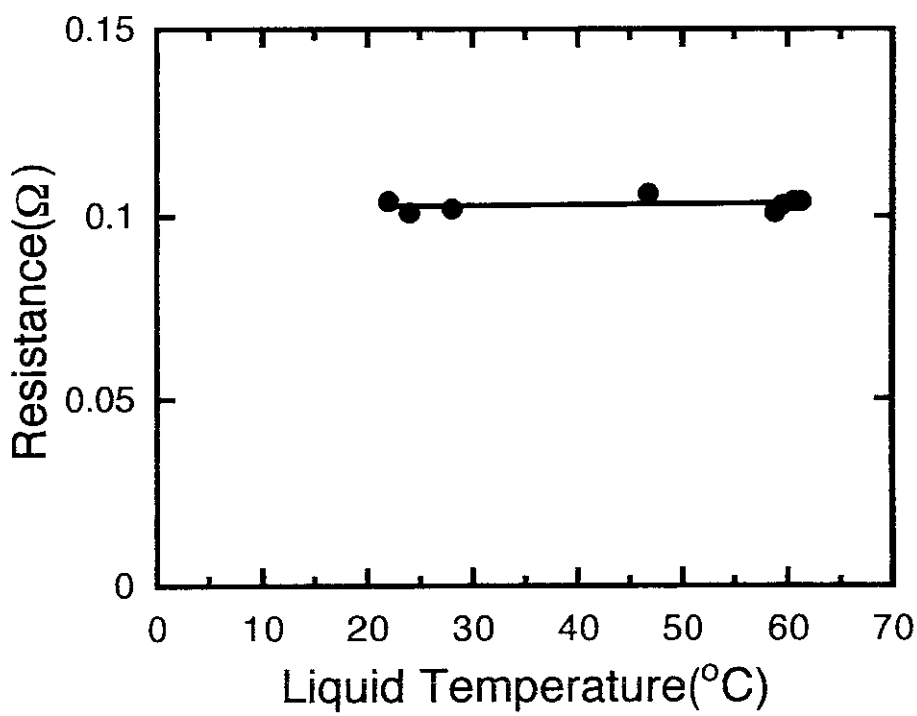
0.15
0.1
0.05
0
Resistance(Ω)
0
10
20
30
40
50
60
70
Liquid Temperature(°C)

Fig. 12

Recent Issues of NIFS Series

NIFS-521 K Ida, S Nishimura, T Minami, K Tanaka, S Okamura, M Osakabe, H Idei, S Kubo, C Takahashi and K Matsuoka,
High Ion Temperature Mode in CHS Heliotron/torsatron Plasmas, Nov 1997

NIFS-522 M. Yokoyama, N Nakajima and M Okamoto,
Realization and Classification of Symmetric Stellarator Configurations through Plasma Boundary Modulations, Dec 1997

NIFS-523 H Kitauchi,
Topological Structure of Magnetic Flux Lines Generated by Thermal Convection in a Rotating Spherical Shell, Dec. 1997

NIFS-524 T Ohkawa,
Tunneling Electron Trap, Dec 1997

NIFS-525 K Itoh, S.-I Itoh, M Yagi, A Fukuyama,
Solitary Radial Electric Field Structure in Tokamak Plasmas, Dec 1997

NIFS-526 Andrey N Lyakhov,
Alfven Instabilities in FRC Plasma, Dec 1997

NIFS-527 J. Uramoto,
Net Current Increment of negative Muonlike Particle Produced by the Electron and Positive Ion Bunch-method; Dec 1997

NIFS-528 Andrey N Lyakhov,
Comments on Electrostastic Drift Instabilities in Field Reversed Configuraiton, Dec 1997

NIFS-529 J Uramoto,
Pair Creation of Negative and Positive Pionlike (Muonlike) Particle by Interaction between an Electron Bunch and a Positive Ion Bunch; Dec. 1997

NIFS-530 J Uramoto,
Measuring Method of Decay Time of Negative Muonlike Particle by Beam Collector Applied RF Bias Voltage; Dec 1997

NIFS-531 J. Uramoto,
Confirmation Method for Metal Plate Penetration of Low Energy Negative Pionlike or Muonlike Particle Beam under Positive Ions; Dec 1997

NIFS-532 J Uramoto,
Pair Creations of Negative and Positive Pionlike (Muonlike) Particle or K Mesonlike (Muonlike) Particle in H2 or D2 Gas Discharge in Magnetic Field; Dec 1997

NIFS-533 S Kawata, C Boonmee, T. Teramoto, L Drska, J. Limpouch, R. Liska, M Sinor,
Computer-Assisted Particle-in-Cell Code Development;Dec 1997

NIFS-534 Y Matsukawa, T. Suda, S Ohnuki and C Namba,
Microstructure and Mechanical Property of Neutron Irradiated TiNi Shape Memory Alloy; Jan. 1998

NIFS-535 A. Fujisawa, H Iguchi, H. Idei, S. Kubo, K. Matsuoka, S Okamura, K Tanaka, T Minami, S. Ohdachi, S Morita, H. Zushi, S. Lee, M. Osakabe, R Akiyama, Y. Yoshimura, K Toi, H. Sanuki, K Itoh, A. Shimizu, S Takagi, A Ejiri, C. Takahashi, M. Kojima, S Hidekuma, K. Ida, S Nishimura, N. Inoue, R Sakamoto, S.-I Itoh, Y Hamada, M Fujiwara,
Discovery of Electric Pulsation in a Toroidal Helical Plasma; Jan 1998

NIFS-536 Lj R Hadzievski, M M. Skoric, M Kono and T. Sato,
Simulation of Weak and Strong Langmuir Collapse Regimes; Jan. 1998

NIFS-537 H Sugama, W. Horton,
Nonlinear Electromagnetic Gyrokinetic Equation for Plasmas with Large Mean Flows; Feb 1998

NIFS-538 H Iguchi, T P Crowley, A. Fujisawa, S Lee, K. Tanaka, T Minami, S Nishimura, K Ida, R Akiyama, Y. Hamada, H., Idei, M. Isobe, M Kojima, S. Kubo, S Morita, S. Ohdachi, S Okamura, M. Osakabe, K Matsuoka, C Takahashi and K. Toi,
Space Potential Fluctuations during MHD Activities in the Compact Helical System (CHS); Feb 1998

NIFS-539 Takashi Yabe and Yan Zhang,
Effect of Ambient Gas on Three-Dimensional Breakup in Coronet Formation Process; Feb 1998

NIFS-540 H. Nakamura, K. Ikeda and S. Yamaguchi,
Transport Coefficients of InSb in a Strong Magnetic Field; Feb 1998

NIFS-541 J. Uramoto,
Development of ν_μ Beam Detector and Large Area ν_μ Beam Source by H_2 Gas Discharge (I); Mar. 1998

NIFS-542 J. Uramoto,
Development of bar{ν}$_\mu$ Beam Detector and Large Area bar{ν}$_\mu$ Beam Source by H_2 Gas Discharge (II); Mar. 1998

NIFS-543 J. Uramoto,
Some Problems inside a Mass Analyzer for Pions Extracted from a H_2 Gas Discharge, Mar. 1998

NIFS-544 J. Uramoto,
Simplified ν_μ, bar{ν}$_\mu$ Beam Detector and ν_μ bar{ν}$_\mu$ Beam Source by Interaction between an Electron Bunch and a Positive Ion Bunch; Mar 1998

NIFS-545 J. Uramoto,
Various Neutrino Beams Generated by D_2 Gas Discharge; Mar.1998

NIFS-546 R. Kanno, N. Nakajima, T. Hayashi and M. Okamoto,
Computational Study of Three Dimensional Equilibria with the Bootstrap Current; Mar. 1998

NIFS-547 R. Kanno, N Nakajima and M. Okamoto,
Electron Heat Transport in a Self-Similar Structure of Magnetic Islands; Apr. 1998

NIFS-548 J.E. Rice,
Simulated Impurity Transport in LHD from MIST; May 1998

NIFS-549 M.M. Skonc, T. Sato, A.M. Maluckov and M.S. Jovanovic,
On Kinetic Complexity in a Three-Wave Interaction; June 1998

NIFS-550 S. Goto and S. Kida,
Passive Saclar Spectrum in Isotropic Turbulence: Prediction by the Lagrangian Direct-interaction Approximation; June 1998

NIFS-551 T. Kuroda, H. Sugama, R Kanno, M. Okamoto and W Horton,
Initial Value Problem of the Toroidal Ion Temperature Gradient Mode ; June 1998

NIFS-552 T. Mutoh, R. Kumazawa, T. Seki, F. Simpo, G. Nomura, T. Ido and T Watari,
Steady State Tests of High Voltage Ceramic Feedthoughs and Co-Axial Transmission Line of ICRF Heating System for the Large Helical Device ; June 1998

NIFS-553 N. Noda, K. Tsuzuki, A Sagara, N Inoue, T. Muroga,
oronaization in Future Devices -Protecting Layer against Tritium and Energetic Neutrals-: July 1998

NIFS-554 S. Murakami and H. Saleem,
Electromagnetic Effects on Rippling Instability and Tokamak Edge Fluctuations; July 1998

NIFS-555 H. Nakamura, K Ikeda and S. Yamaguchi,
Physical Model of Nernst Element; Aug. 1998

NIFS-556 H. Okumura, S. Yamaguchi, H. Nakamura, K. Ikeda and K. Sawada,
Numerical Computation of Thermoelectric and Thermomagnetic Effects Aug. 1998

NIFS-557 Y Takeiri, M Osakabe, K Tsumori, Y. Oka, O Kaneko, E Asano, T. Kawamoto, R. Akiyama and M Tanaka,
Development of a High-Current Hydrogen-Negative Ion Source for LHD-NBI System; Aug.1998

NIFS-558 M Tanaka, A Yu Grosberg and T Tanaka
Molecular Dynamics of Structure Organization of Polyampholytes Sep 1998

NIFS-559 R Horiuchi K Nishimura and T Watanabe
Kinetic Stabilization of Tilt Disruption in Field Reversed Configurations Sep 1998
(IAEA-CN-69/THP1/11)

NIFS-560 S Sudo, K Kholopenkov K. Matsuoka, S Okamura C Takahashi, R Akiyama A Fujisawa, K Ida, H Idei H Iguchi, M Isobe S Kado, K Kondo, S Kubo, H Kuramoto, T Minami S Morita, S Nishimura, M Osakabe, M Sasao, B Peterson, K Tanaka, K Toi and Y Yoshimura,
Particle Transport Study with Tracer-Encapsulated Solid Pellet Injection, Oct 1998
(IAEA-CN-69/EXP1/18)

NIFS-561 A. Fujisawa, H Iguchi, S Lee, K Tanaka, T Minami, Y Yoshimura, M Osakabe, K Matsuoka, S Okamura, H Idei, S Kubo, S Ohdachi, S Morita, R Akiyama, K Toi, H. Sanuki, K Itoh, K Ida, A. Shimizu, S Takagi, C Takahashi, M. Kojima, S Hidekuma, S Nishimura, M Isobe, A Ejiri, N Inoue, R Sakamoto, Y Hamada and M Fujiwara,
Dynamic Behavior Associated with Electric Field Transitions in CHS Heliotron/Torsatron, Oct 1998
(IAEA-CN-69/EX5/1)

NIFS-562 S Yoshikawa,
Next Generation Toroidal Devices, Oct 1998

NIFS-563 Y Todo and T Sato,
Kinetic-Magnetohydrodynamic Simulation Study of Fast Ions and Toroidal Alfvén Eigenmodes, Oct 1998
(IAEA-CN-69/THP2/22)

NIFS-564 T. Watari, T Shimozuma, Y Takeiri, R Kumazawa, T Mutoh, M Sato, O Kaneko, K Ohkubo, S Kubo, H Idei, Y Oka, M Osakabe, T Seki, K Tsumori, Y Yoshimura, R Akiyama, T Kawamoto, S Kobayashi, F Shimpo, Y Takita, E Asano, S Itoh, G Nomura, T. Ido, M. Hamabe, M. Fujiwara, A Iiyoshi, S Morimoto, T Bigelow and Y P Zhao,
Steady State Heating Technology Development for LHD, Oct 1998
(IAEA-CN-69/FTP/21)

NIFS-565 A Sagara, K Y. Watanabe, K Yamazaki, O Motojima, M Fujiwara, O. Mitarai, S Imagawa, H Yamanishi, H Chikaraishi, A Kohyama, H Matsui, T Muroga, T. Noda, N. Ohyabu, T Satow, A.A Shishkin, S Tanaka, T. Terai and T Uda,
LHD-Type Compact Helical Reactors, Oct 1998
(IAEA-CN-69/FTP/03(R)

NIFS-566 N Nakajima, J. Chen, K. Ichiguchi and M Okamoto,
Global Mode Analysis of Ideal MHD Modes in L=2 Heliotron/Torsatron Systems, Oct 1998
(IAEA-CN-69/THP1/08)

NIFS-567 K Ida, M. Osakabe, K. Tanaka, T Minami, S Nishimura, S Okamura, A. Fujisawa, Y Yoshimura, S Kubo, R Akiyama, D S.Darrow, H. Idei, H. Iguchi, M Isobe, S. Kado, T Kondo, S. Lee, K Matsuoka, S Morita, I. Nomura, S. Ohdachi, M Sasao, A. Shimizu, K. Tumori, S. Takayama, M Takechi, S. Takagi, C Takahashi, K Toi and T Watari,
Transition from L Mode to High Ion Temperature Mode in CHS Heliotron/Torsatron Plasmas; Oct 1998
(IAEA-CN-69/EX2/2)

NIFS-568 S. Okamura, K. Matsuoka, R Akiyama, D S Darrow, A Ejiri, A Fujisawa, M Fujiwara, M Goto, K. Ida H Idei, H Iguchi, N Inoue, M Isobe, K. Itoh, S Kado, K. Khlopenkov, T. Kondo, S Kubo, A Lazaros, S Lee, G Matsunaga, T Minami, S Morita, S Murakami, N. Nakajima, N Nikai, S Nishimura, I. Nomura, S Ohdachi, K. Ohkuni, M. Osakabe, R Pavlichenko, B Peterson, R Sakamoto, H. Sanuki, M. Sasao, A Shimizu, Y. Shirai, S Sudo, S Takagi, C. Takahashi, S. Takayama, M. Takechi, K Tanaka, K. Toi, K Yamazaki, Y Yoshimura and T. Watari,
Confinement Physics Study in a Small Low-Aspect-Ratio Helical Device CHS, Oct 1998
(IAEA-CN-69/OV4/5)

NIFS-569 M.M. Skoric, T. Sato, A Maluckov, M.S. Jovanovic,
Micro- and Macro-scale Self-organization in a Dissipative Plasma; Oct 1998

NIFS-570 T. Hayashi, N Mizuguchi, T-H. Watanabe, T Sato and the Complexity Simulation Group
Nonlinear Simulations of Internal Reconnection Event in Spherical Tokamak, Oct 1998
(IAEA-CN-69/TH3/3)

NIFS-571 A. Iiyoshi, A Komori, A. Ejiri, M. Emoto, H Funaba, M Goto, K Ida, H Idei, S Inagaki, S. Kado, O Kaneko, K Kawahata, S Kubo, R. Kumazawa, S. Masuzaki T Minami, J. Miyazawa, T Morisaki, S Morita, S Murakami, S. Muto, T Muto, Y Nagayama, Y. Nakamura, H. Nakanishi, K Nanhara, K. Nishimura, N Noda, T Kobuchi, S. Ohdachi, N Ohyabu, Y Oka, M Osakabe, T Ozaki, B J Peterson, A Sagara, S Sakakibara, R Sakamoto, H Sasao, M Sasao, K Sato, M Sato, T Seki, T. Shimozuma, M Shoji, H Suzuki, Y Takeiri, K Tanaka, K Toi, T Tokuzawa, K Tsumori, I Yamada, H Yamada, S. Yamaguchi, M Yokoyama, K Y Watanabe, T. Watari, R Akiyama, H Chikaraishi, K Haba, S Hamaguchi, S Iima, S Imagawa, N Inoue, K Iwamoto, S Kitagawa, Y Kubota, J Kodaira, R Maekawa, T Mito T Nagasaka, A Nishimura, Y. Takita, C Takahashi, K Takahata, K Yamauchi, H Tamura, T Tsuzuki, S Yamada, N Yanagi, H Yonezu, Y Hamada, K Matsuoka, K Murai, K. Ohkubo, I. Ohtake, M Okamoto, S Sato, T Satow, S Sudo, S Tanahashi, K. Yamazaki, M. Fujiwara and O Motojima,
An Overview of the Large Helical Device Project, Oct 1998

(IAEA-CN-69/OV1/4)

NIFS-572 M. Fujiwara, H. Yamada, A. Ejiri, M Emoto, H Funaba, M Goto, K. Ida, H Idei, S. Inagaki, S. Kado, O. Kaneko, K Kawahata, A. Komori, S. Kubo, R. Kumazawa, S. Masuzaki, T. Minami, J. Miyazawa, T. Morisaki, S. Morita, S. Murakami, S. Muto, T Muto, Y. Nagayama, Y. Nakamura, H. Nakanishi, K. Narihara, K. Nishimura, N. Noda, T. Kobuchi, S. Ohdachi, N. Ohyabu, Y. Oka, M. Osakabe, T. Ozaki, B. J. Peterson, A. Sagara, S. Sakakibara, R. Sakamoto, H. Sasao, M. Sasao, K. Sato, M. Sato, T. Seki, T. Shimozuma, M. Shoji, H. Sazuki, Y. Takeiri, K. Tanaka, K. Toi, T. Tokuzawa, K. Tsumori, I. Yamada, S. Yamaguchi, M. Yokoyama, K.Y. Watanabe, T. Watari, R. Akiyama, H. Chikaraishi, K. Haba, S. Hamaguchi, M. Iima, S. Imagawa, N. Inoue, K. Iwamoto, S. Kitagawa, Y. Kubota, J. Kodaira, R. Maekawa, T. Mito, T Nagasaka, A. Nishimura, Y. Takita, C. Takahashi, K. Takahata, K. Yamauchi, H. Tamura, T. Tsuzuki, S. Yamada, N Yanagi, H. Yonezu, Y. Hamada, K. Matsuoka, K. Murai, K. Ohkubo, I. Ohtake, M. Okamoto, S. Sato, T. Satow, S. Sudo, S. Tanahashi, K. Yamazaki, O. Motojima and A. Iiyoshi,
Plasma Confinement Studies in LHD; Oct. 1998
(IAEA-CN-69/EX2/3)

NIFS-573 O. Motojima, K. Akaishi, H. Chikaraishi, H. Funaba, S. Hamaguchi, S. Imagawa, S. Inagaki, N. Inoue, A. Iwamoto, S. Kitagawa, A. Komori, Y Kubota, R. Maekawa, S. Masuzaki, T. Mito, J Miyazawa, T Morisaki, T Muroga, T Nagasaka, Y. Nakmura, A. Nishimura, K. Nishimura, N. Noda, N. Ohyabu, S. Sagara, S Sakakibara, R Sakamoto, S Satoh, T. Satow, M Shoji, H Suzuki, K. Takahata, H. Tamura, K. Watanabe, H. Yamada, S Yamada, S Yamaguchi, K Yamazaki, N. Yanagi, T Baba, H. Hayashi, M. Iima, T. Inoue, S. Kato, T. Kato, T. Kondo, S. Moriuchi, H Ogawa, I Ohtake, K. Ooba, H. Sekiguchi, N Suzuki, S. Takami, Y Taniguchi, T. Tsuzuki, N. Yamamoto, K. Yasui, H. Yonezu, M. Fujiwara and A. Iiyoshi,
Progress Summary of LHD Engineering Design and Construction; Oct. 1998
(IAEA-CN-69/FT2/1)

NIFS-574 K. Toi, M. Takechi, S. Takagi, G. Matsunaga, M. Isobe, T. Kondo, M Sasao, D S Darrow, K. Ohkuni, S. Ohdachi, R. Akiyama A. Fujisawa, M. Gotoh, H. Idei, K. Ida, H. Iguchi, S. Kado, M. Kojima, S. Kubo, S. Lee, K. Matsuoka, T. Minami, S. Morita, N. Nikai, S Nishimura, S. Okamura, M. Osakabe, A. Shimizu, Y. Shirai, C. Takahashi, K. Tanaka, T. Watari and Y. Yoshimura,
Global MHD Modes Excited by Energetic Ions in Heliotron/Torsatron Plasmas;Oct 1998
(IAEA-CN-69/EXP1/19)

NIFS-575 Y Hamada, A. Nishizawa, Y Kawasumi, A Fujisawa, M. Kojima, K Narihara, K. Ida, A. Ejiri, S Ohdachi, K. Kawahata, K Toi, K Sato, T Seki, H. Iguchi, K. Adachi, S Hidekuma, S.Hirokura, K. Iwasaki, T Ido, R Kumazawa, H Kuramoto, T. Minami, I.. Nomura, M. Sasao, K.N. Sato, T. Tsuzuki, I. Yamada and T. Watari,
Potential Turbulence in Tokamak Plasmas;Oct. 1998
(IAEA-CN-69/EXP2/14)

NIFS-576 S. Murakami, U. Gasparino, H. Idei, S. Kubo, H. Maassberg, N Marushchenko, N. Nakajima, M. Romé and M Okamoto,
5D Simulation Study of Suprathermal Electron Transport in Non-Axisymmetric Plasmas;Oct 1998
(IAEA-CN-69/THP1/01)

NIFS-577 S. Fujiwara and T. Sato,
Molecular Dynamics Simulation of Structure Formation of Short Chain Molecules; Nov. 1998

NIFS-578 T. Yamagishi,
Eigenfunctions for Vlasov Equation in Multi-species Plasmas Nov. 1998

NIFS-579 M. Tanaka, A. Yu Grosberg and T. Tanaka,
Molecular Dynamics of Strongly-Coupled Multichain Coulomb Polymers in Pure and Salt Aqueous Solutions;Nov. 1998

NIFS-580 J Chen, N Nakajima and M. Okamoto,
Global Mode Analysis of Ideal MHD Modes in a Heliotron/Torsatron System: I. Mercier-unstable Equilibria;Dec 1998

NIFS-581 M. Tanaka, A. Yu Grosberg and T. Tanaka,
Comparison of Multichain Coulomb Polymers in Isolated and Periodic Systems: Molecular Dynamics Study; Jan 1999

NIFS-582 V.S. Chan and S. Murakami,
Self-Consistent Electric Field Effect on Electron Transport of ECH Plasmas; Feb. 1999

NIFS-583 M. Yokoyama, N. Nakajima, M. Okamoto, Y. Nakamura and M. Wakatani,
Roles of Bumpy Field on Collisionless Particle Confinement in Helical-Axis Heliotrons;Feb. 1999

NIFS-584 T.-H. Watanabe, T. Hayashi, T. Sato, M. Yamada and H. Ji,
Modeling of Magnetic Island Formation in Magnetic Reconnection Experiment, Feb 1999

NIFS-585 R. Kumazawa, T. Mutoh, T. Seki, F. Shinpo, G. Nomura, T. Ido, T. Watari, Jean-Marie Noterdaeme and Yangping Zhao,
Liquid Stub Tuner for Ion Cyclotron Heating;Mar. 1999